COBEM 2023 27TH INTERNATIONAL CONGRESS OF MECHANICAL ENGENEERING

ABCM Brazilian Society of Mechanical Sciences and Engineering
27th ABCM International Congress of Mechanical Engineering
December 04-08, 2023, Florianópolis-SC, Brazil

COB-2023-0105
FULL ISOTROPIC YIELD SURFACES FOR POROUS DUCTILE MATERIALS BY COMPUTATIONAL HOMOGENIZATION

Wanderson Ferreira dos Santos
Ayrton Ribeiro Ferreira
Sergio Persival Baroncini Proença
Department of Structural Engineering, Sao Carlos School of Engineering, University of Sao Paulo. Address: Av. Trab. Sao Carlense, 400, Zip-Code: 13566-590, Sao Carlos, Sao Paulo, Brazil
e-mails: wanderson_santos@usp.br, ayrton.f01@gmail.com, persival@sc.usp.br

Abstract. *The formulation of realistic macroscopic constitutive models for porous elasto-plastic solids requires consideration of the effects of voids on the distribution of stresses and strains at the microscale. In this context, a computational homogenization procedure is explored herein to investigate yield criteria for porous ductile media. The microscale of the porous solid is modeled using the concept of Representative Volume Element (RVE). The microscopic fields of the RVE are computed by three-dimensional (3D) simulations using the Finite Element Method with the hypothesis of small strains. Macroscopic strain and stress fields are then obtained based on the volume averaging of the microscopic strain and stress fields over the RVE. Different stress states are imposed on the RVEs, encompassing low, intermediate, and high triaxilities. In particular, the sensitivity of the yield criterion to the Lode angle is investigated by combining shear states with low and intermediate triaxialities. The influence of the RVE void morphology is assessed on the yield surfaces, considering the uniform strain boundary condition and the periodic boundary condition imposed on the RVEs. Spherical and cubic voids are investigated for a cubic RVE, and the results provide reference limits for voids with similar morphology. The RVE matrix behavior is adopted as an isotropic perfect elasto-plastic material following the von Mises yield criterion. In general, the yield surfaces have different geometries, resulting in different constitutive behaviors for the same load situations. The responses provided by the periodic boundary condition show significant differences when compared to the uniform strain boundary condition. Moreover, the stress Lode angle has a strong influence on the yield surface geometry.*

Keywords: *porous ductile solids, full yield surfaces, computational homogenization, void morphology, boundary conditions.*

1. INTRODUCTION

Several analytical, semi-analytical and numerical works have been developed in the context of yield surfaces for porous ductile media. Gurson analytical model is well known in the literature, in which Gurson (1977) proposed a yield criterion for ductile porous media by means of the Limit Analysis theory and concepts of average-based homogenization. The spherical cell has a rigid-perfectly plastic matrix with a centered spherical void.

In a more recent context, approaches based on computational homogenization have been successfully applied to estimate the plastic surfaces of porous ductile solids. Some works in this direction are briefly discussed below.

Fritzen *et al.* (2012) investigated yield surfaces for porous elasto-plastic materials by a 3D computational homogenization strategy based on Monte Carlo numerical simulations. RVEs with spherical voids randomly distributed in the ductile matrix were simulated, imposing different boundary conditions on the RVE boundary. The computational results were compared to analytical models, and an extension for the Gurson–Tvergaard–Needleman model was proposed.

Khdir *et al.* (2015) presented a 3D computational homogenization study to assess the effect of void shape and void content on the overall yield surface of random porous media. The cited work was an extension of Fritzen *et al.* (2012) in order to investigate the case of random porous media containing non-spherical voids. In particular, elasto-plastic media with oblate and prolate spheroidal voids were numerically simulated by Khdir *et al.* (2015). The final results were compared with some Gurson-type yield criteria. The computational results showed good agreement with the model recently proposed by Fritzen *et al.* (2012).

Carvalho *et al.* (2018) proposed a 3D computational homogenization strategy to predict the yielding behavior of ductile porous materials using three-dimensional finite element models under the geometrically nonlinear hypothesis of finite strains. In particular, the effect of void morphology was addressed by simulating RVEs with single-centered ellipsoidal voids. Different kinematic models were imposed on RVEs: linear boundary displacements (upper bound); boundary displacement fluctuation periodicity; and uniform boundary traction (lower bound). The results showed that analytical models usually overestimate the effect of void morphology on the yield locus.

Dæhli *et al.* (2019) investigated yield surfaces for porous ductile solids by numerical limit analyses using a 3D finite

element model. The study was focused on the numerical simulation of a spherical void centered on a spherical unit cell with a Hershey-Hosford matrix yield function. The approach allowed the investigation of porous ductile solids with a matrix yield function dependent on the second and third deviatoric stress invariants.

Recently, Santos *et al.* (2022) explored an approach based on 3D computational homogenization to investigate the effect of void morphology on yield surfaces of isotropic porous ductile media. More specifically, spherical and cubic voids were simulated under the uniform strain boundary condition for purposes of comparison with the Gurson model. Spherical and cubic voids are interesting because the yield surfaces may provide reference limits for other voids with similar morphology. Yield surfaces with complete geometry were obtained from the computational approach, in which surfaces can be represented in the meridional and deviator planes. Furthermore, the effect of the Lode angle can be evaluated more clearly. It is worth mentioning that the complete geometric representation requires a high computational cost. The results of numerical limit analyzes present significant differences in comparison with Gurson's analytical model.

In this context, this work is an extension of Santos *et al.* (2022) in order to assess the influence of the boundary condition on the complete yield surfaces for isotropic porous ductile solids. RVEs with cubic and spherical voids (centered in the ductile matrix) are investigated. The main novelty is the incorporation of the periodic boundary condition in the numerical simulation of the RVEs. Furthermore, the ductile matrix is governed by the von Mises model and the hypothesis of small strains is assumed. Numerous numerical simulations were performed to create the complete plastic surfaces (meridional and deviatoric planes), considering low, intermediate, and high triaxiality rates.

2. SOME PRELIMINARY CONCEPTS

In this section, some preliminary concepts are briefly presented on average-based homogenization theory and boundary conditions.

2.1 Average-based homogenization theory

Average-based homogenization theories are interesting strategies to obtain the homogenized constitutive behavior of non-homogeneous media. In general, the macroscopic behavior is obtained by modeling the phenomena observed at lower scales. In particular, Fig. 1 presents two observation scales for a porous material: (i) a macroscopic scale (or macro-continuum); and (ii) a microscopic scale, which is often modeled with the concept of unit cell or RVE.

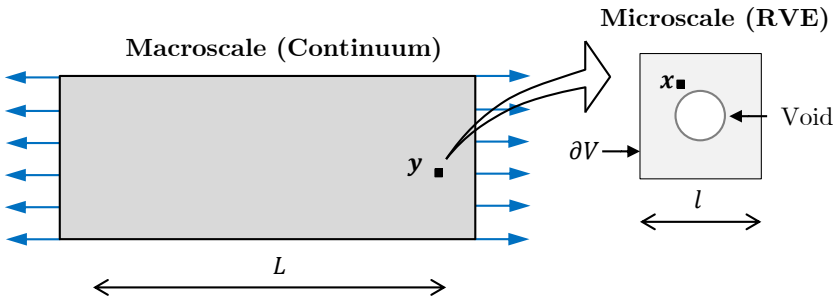

Figure 1: Illustrative scheme of macroscale (continuum) and microscale (RVE), in which $l << L$.

In this context, the strain and stress tensors ($\boldsymbol{E}$ and $\boldsymbol{\Sigma}$) at an arbitrary material point $\boldsymbol{y}$ of the continuum are, respectively, the volume average of the strain and stress tensors ($\boldsymbol{\varepsilon}$ and $\boldsymbol{\sigma}$) over a local RVE (Bishop and Hill, 1951):

$$\boldsymbol{E}(\boldsymbol{y}) =< \boldsymbol{\varepsilon}(\boldsymbol{x}) >= \frac{1}{V}\int_V \boldsymbol{\varepsilon}(\boldsymbol{x})dV, \tag{1}$$

$$\boldsymbol{\Sigma}(\boldsymbol{y}) =< \boldsymbol{\sigma}(\boldsymbol{x}) >= \frac{1}{V}\int_V \boldsymbol{\sigma}(\boldsymbol{x})dV, \tag{2}$$

where $< \cdot >$ indicates the volume average of the microscopic fields over the RVE; and V is the initial volume of the RVE.

The Hill Mandel principle is important for understanding the association between macro and micro scales. In summary, this principle establishes that the macroscopic stress power must equal the volume average of the microscopic stress power over the RVE (Bishop and Hill, 1951; Mandel, 1971):

$$\boldsymbol{\Sigma} : \boldsymbol{E} = \frac{1}{V}\int_V \boldsymbol{\sigma} : \boldsymbol{\varepsilon} dV =< \boldsymbol{\sigma} : \boldsymbol{\varepsilon} > . \tag{3}$$

2.2 Boundary conditions

The macroscopic constitutive behavior requires the solution of a Boundary Value Problem (BVP) for the RVE. In the context of the present work, two well-known boundary conditions in the literature are described in the following (see Fig. 2): (i) uniform strain boundary condition (USBC); and (ii) the periodic boundary condition (PBC).

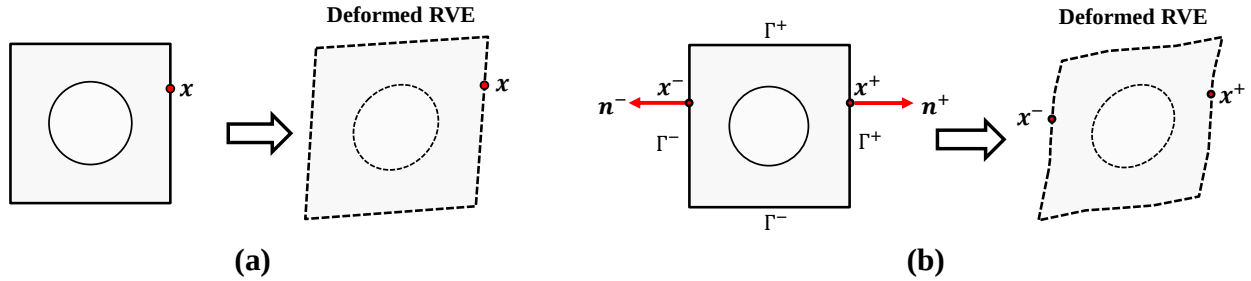

Figure 2: Illustrative representation of: (a) Uniform strain boundary condition; (b) Periodic boundary condition.

2.2.1 Uniform strain boundary condition

The uniform strain boundary condition (USBC) is given by:

$$\boldsymbol{u} = \boldsymbol{E}^* \cdot \boldsymbol{x} \quad \forall \quad \boldsymbol{x} \in \partial V, \tag{4}$$

where $\boldsymbol{u}$ is the displacement field; $\boldsymbol{E}^*$ is the macroscopic homogeneous strain tensor imposed on the outer contour of the RVE; and $\boldsymbol{x}$ is the position vector. Moreover, after some deductions, we can prove that $\boldsymbol{E} =< \boldsymbol{\varepsilon} >= \boldsymbol{E}^*$.

2.2.2 Periodic boundary condition

The periodic boundary condition (PBC) is given by:

$$\boldsymbol{u} = \boldsymbol{E}^* \cdot \boldsymbol{x} + \tilde{\boldsymbol{u}} \quad \forall \quad \boldsymbol{x} \in \partial V, \tag{5}$$

where $\tilde{\boldsymbol{u}}$ is called periodic fluctuation. In this case, we can also prove that $\boldsymbol{E} =< \boldsymbol{\varepsilon} >= \boldsymbol{E}^*$.

Furthermore:

$$\boldsymbol{\sigma} \cdot \boldsymbol{n}^+ = \boldsymbol{\sigma} \cdot \boldsymbol{n}^- \quad \forall \quad \boldsymbol{x} \in \partial V, \tag{6}$$

with the unit normals obeying $\boldsymbol{n}^+ = -\boldsymbol{n}^-$.

Note that $\tilde{\boldsymbol{u}}$ is not known initially in the problem. An alternative for applying the periodic condition is to divide the RVE contour into positive (Γ^+) and negative parts (Γ^-). Thus, each point $\boldsymbol{x}^+$ on Γ^+ has a corresponding point $\boldsymbol{x}^-$ on Γ^-. Consequently, the displacements $\boldsymbol{u}^+$ and $\boldsymbol{u}^-$ are given by:

$$\boldsymbol{u}^+ = \boldsymbol{E}^* \cdot \boldsymbol{x}^+ + \tilde{\boldsymbol{u}}(\boldsymbol{x}^+), \tag{7a}$$

$$\boldsymbol{u}^- = \boldsymbol{E}^* \cdot \boldsymbol{x}^- + \tilde{\boldsymbol{u}}(\boldsymbol{x}^-). \tag{7b}$$

In this sense, each boundary point on the positive side ($\boldsymbol{x}^+$) can be associated with another boundary point on the negative side ($\boldsymbol{x}^-$):

$$\boldsymbol{u}^+ - \boldsymbol{u}^- = \boldsymbol{E}^* \cdot \left(\boldsymbol{x}^+ - \boldsymbol{x}^-\right). \tag{8}$$

Therefore, the periodic boundary condition can be imposed by constraint equations added in the BVP for the RVE.

3. METHODOLOGY TO OBTAIN THE YIELD SURFACES

In this section, the methodology to obtain the yield surfaces is presented. Initially, the geometric representation of the isotropic yield surface is shown. Afterward, some aspects of the numerical simulations are described, including the RVE morphologies and the loading program imposed on the RVE. Finally, the computational homogenization process explored in this work is shown.

3.1 Geometric representation of macroscopic yield surfaces

In this work, the yield surfaces of porous ductile media are represented in the meridional and deviator planes, in which cuts are conveniently performed on the three-dimensional surfaces (see Fig. 3). In this sense, mechanical invariants help in the representation and interpretation of surface results.

The macroscopic stress tensor ($\boldsymbol{\Sigma}$) can be defined in terms of its mechanical invariants (Benallal *et al.*, 2014): (i) Σ_m (hydrostatic stress or mean strain); (ii) Σ_{eq} (von Mises stress or equivalent stress); (iii) Θ (stress Lode angle). In this context:

$$\boldsymbol{\Sigma} = \frac{2}{3}\Sigma_{eq}\boldsymbol{e}'(\Theta) + \Sigma_m \mathbf{I}, \tag{9}$$

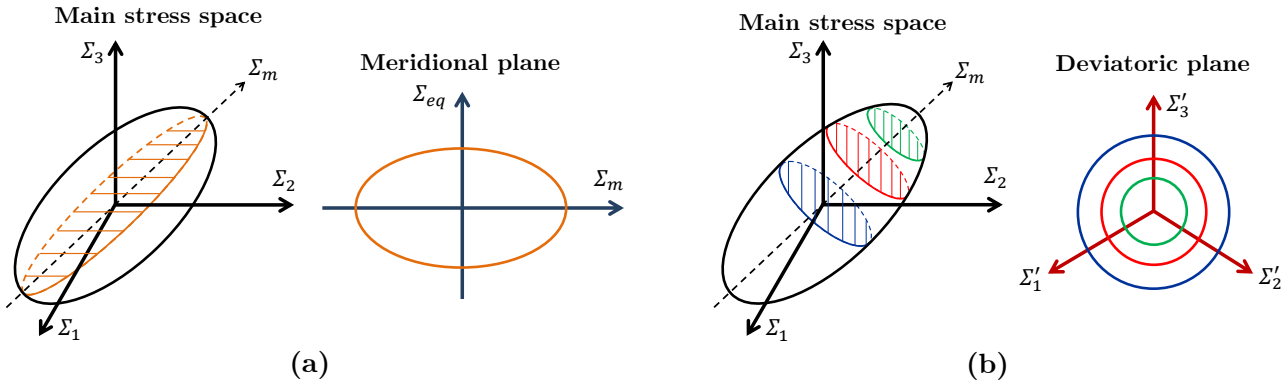

Figure 3: Yield surfaces for a porous material: (a) meridional plane; (b) diverter plane. Adapted from Santos (2021).

where

$$\Sigma_m = \frac{1}{3}\,\mathrm{Tr}\,(\boldsymbol{\Sigma})\,, \quad \boldsymbol{\Sigma}' = \boldsymbol{\Sigma} - \Sigma_m \mathbf{I},$$

$$\Sigma_{eq} = \sqrt{\frac{3}{2}\boldsymbol{\Sigma}' : \boldsymbol{\Sigma}'},$$

$$\boldsymbol{e}'(\Theta) = \begin{bmatrix} \cos\Theta & 0 & 0 \\ 0 & \cos\left(\Theta - \dfrac{2\pi}{3}\right) & 0 \\ 0 & 0 & \cos\left(\Theta + \dfrac{2\pi}{3}\right) \end{bmatrix},$$

$$\Theta = \frac{1}{3}\arccos\left(\frac{27}{2}\frac{\det \boldsymbol{\Sigma}'}{\Sigma_{eq}^3}\right),$$

where $\mathbf{I}$ is the nomenclature for the second order unity tensor.

Introducing the concept of stress triaxiality ratio ($T = \Sigma_m/\Sigma_{eq}$), Eq. (9) is rewritten as:

$$\boldsymbol{\Sigma} = \Sigma_{eq}\left[\frac{2}{3}\boldsymbol{e}'(\Theta) + T\mathbf{I}\right]. \tag{10}$$

As shown in Fig. 4, the mechanical invariants have meaning in the graphic representation of yield surfaces.

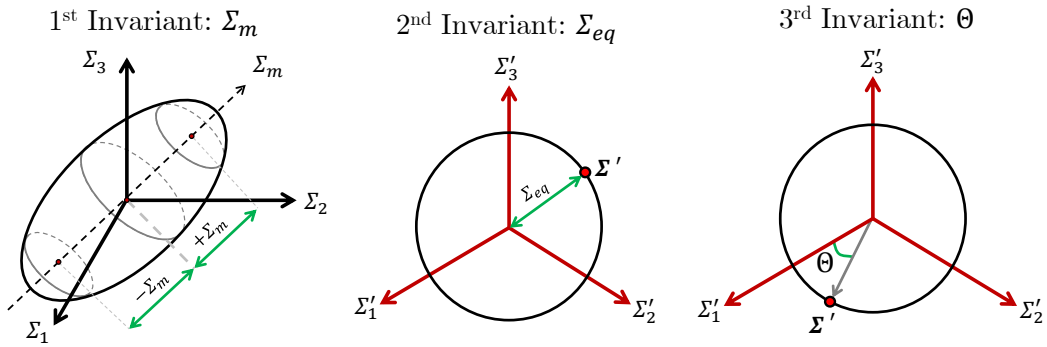

Figure 4: Illustrative representation of mechanical invariants for stress. Adapted from Santos (2021).

In a similar way, the macroscopic strain tensor ($\boldsymbol{E}$) can be defined in terms of its mechanical invariants (Benallal et al., 2014): (i) E_m (hydrostatic strain or mean strain); (ii) E_{eq} (von Mises strain or equivalent strain); (iii) η (strain Lode angle). In this case:

$$\boldsymbol{E} = E_{eq}\boldsymbol{e}'(\eta) + E_m\mathbf{I}, \tag{11}$$

where

$$E_m = \frac{1}{3}\,\mathrm{Tr}\,(\boldsymbol{E})\,, \quad \boldsymbol{E}' = \boldsymbol{E} - E_m\mathbf{I},$$

$$E_{eq} = \sqrt{\frac{2}{3}\boldsymbol{E}' : \boldsymbol{E}'},$$

$$\boldsymbol{e}'(\eta) = \begin{bmatrix} \cos\eta & 0 & 0 \\ 0 & \cos\left(\eta - \frac{2\pi}{3}\right) & 0 \\ 0 & 0 & \cos\left(\eta + \frac{2\pi}{3}\right) \end{bmatrix},$$

$$\eta = \frac{1}{3}\arccos\left(\frac{4\det \boldsymbol{E}'}{E_{eq}^3}\right).$$

Using the concept of strain triaxiality ratio ($H = E_m/E_{eq}$), Eq. (11) can be rewritten as:

$$\boldsymbol{E} = E_{eq}\left[\boldsymbol{e}'(\eta) + H\mathbf{I}\right]. \tag{12}$$

3.2 Numerical analysis

The study aims to evaluate the influence of void morphology on yield surfaces for isotropic porous ductile media. A porosity (f) of 0.01 is assumed for RVEs. It is worth mentioning that the critical porosity may vary 1% and 2% for most ductile rupture conditions. In this context, two RVE morphologies are numerically simulated: (i) cube with a centered spherical void; (ii) cube with a centered cubic void. Numerical simulations are performed with the 20-node hexahedron element and reduced integration. The finite element meshes are shown in Fig. 5. A mesh refinement study was carried out previously. Furthermore, the propagation of errors in different directions is reduced due to the structured meshes. The matrix is governed by the von Mises model with perfect elasto-plastic behavior. The parameter values of the elasto-plastic simulations are $Y = 2000$ GPa (Young's Modulus), $\nu = 0.499$ (Poisson's ratio) and $\sigma_0 = 500$ MPa (yield stress). The incompressibility hypothesis ($\nu \approx 1/2$) contributes to the minimization of numerical instabilities in some simulations (Daehli et al., 2019). Since our approach is based on the Kinematic Theorem of Limit Analysis, the loading capacity of the RVE is independent on the elastic parameters.

Figure 5: RVE mesh: (a) cube with spherical void (7200 elements); (b) cube with cubic void (7200 elements).

In this work, both uniform and periodic boundary conditions are imposed on the RVE. As presented in subsection 2.1, the homogeneous macroscopic strain tensor ($\boldsymbol{E}$) must be imposed on the RVE. More specifically, we prescribe $\boldsymbol{E}^*$ by Eq. (12). Therefore, the strain Lode angle (η) and the strain rate triaxiality (H) must be defined.

This work addresses isotropic porous ductile media and the yield surface have six-fold symmetry. This allows us to define values of η only in the range between $[0, \pi/3]$. Furthermore, the remaining range $[\pi/3, 2\pi]$ can be conveniently supplemented from the initial results. In this sense, the analyses were computed with 13 values of η equally spaced in the interval $[0, \pi/3]$.

The values for H were defined from Gurson (1977), in which points with approximately equal spacing were selected on the Gurson surface. Then, 51 values of H are defined for the porosity of 0.01. Moreover, the following strategy was adopted to facilitate the application of triaxialities tending to infinity:

$$\tilde{\boldsymbol{E}}^* = \frac{\boldsymbol{E}^*}{||\boldsymbol{E}^*||} = \sqrt{\frac{2}{3}\left(1 - 3\tilde{H}^2\right)}e'(\eta) + \tilde{H}\mathbf{I}, \tag{13}$$

where $\tilde{\boldsymbol{E}}$ is the adjusted macroscopic strain and $\tilde{H}$ is the adjusted strain triaxiality given by:

$$\tilde{H} = \frac{H}{\sqrt{\frac{3}{2} + 3H^2}}, \tag{14}$$

with

$$\lim_{H\to\pm\infty}\tilde{H}=\pm\frac{1}{\sqrt{3}}\quad\text{and}\quad\lim_{H\to 0}\tilde{H}=0. \tag{15}$$

In summary, RVEs were simulated considering two boundary conditions, 71 values for H and 13 values for η. Therefore, 3692 non-linear numerical simulations were computed to obtain the yield surfaces.

3.3 Computational homogenization procedure

The homogenized response is computationally obtained from the microscopic fields calculated by finite elements. In each case, the homogenized macroscopic stress is computed by using the following expression considering all finite elements (N_{elem}):

$$\boldsymbol{\Sigma}=\frac{1}{V}\sum_{i=1}^{N_{\text{elem}}}\boldsymbol{\sigma}_i V_i, \tag{16}$$

where $\boldsymbol{\Sigma}$ is the computationally homogenized stress tensor; $\boldsymbol{\sigma}_i$ is the average stress in the element i computed at their integration points; V_i is the volume of the element i; and V is the total volume of the RVE. Furthermore, the macroscopic homogenized strain is given by $\boldsymbol{E}=\boldsymbol{E}^*$.

4. RESULTS AND DISCUSSION

The complete yield surfaces in the main stress space are shown in Fig. 6. Representations in the meridional and deviator planes can be created by interpolation of the plastic surfaces in Fig. 6. In this work, a linear interpolation was performed using libraries available in the Python programming language. In the deviatoric plane, the cuts are obtained for different values of $C_f\Sigma_m^f$, where C_f is a coefficient and $\Sigma_m^f=-2/3\sigma_0\ln(f)$ is the solution of the Gurson (1977) for triaxiality tending to infinity. The coefficient $C_f\in[0;1]$, where $C_f\to 0$ corresponds to $T\to 0$ and $C_f\to 1$ corresponds to $T\to\infty$. Furthermore, the results are discussed into two parts: (i) influence of void morphology on the yield surfaces for the same boundary condition; (ii) effect of the boundary condition on the yield surfaces for the same RVE.

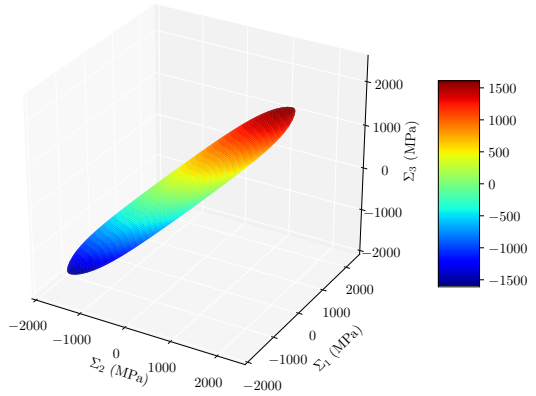

(a) Cubic RVE with a centered spherical void under uniform strain boundary condition (CS-U).

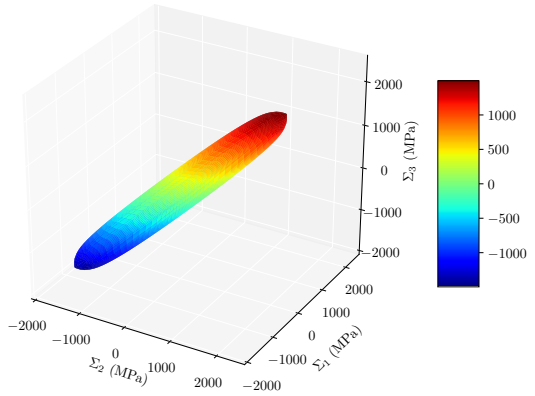

(b) Cubic RVE with a centered spherical void under periodic boundary condition (CS-P).

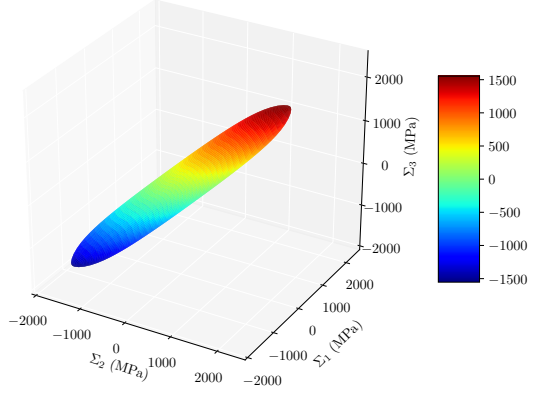

(c) Cubic RVE with a centered cubic void under uniform strain boundary condition (CC-U).

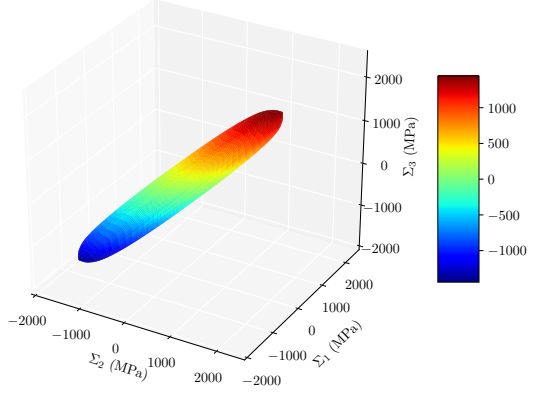

(d) Cubic RVE with a centered cubic void under periodic boundary condition (CC-P).

Figure 6: Yield surfaces in the main stress space (Σ_1, Σ_2 and Σ_3) for $f=0.01$.

4.1 Yield surfaces: influence of the void morphology

Comparisons of yield surfaces for different void morphologies of the RVE under USBC are shown in Fig. 7. On the other hand, a comparison of yield surfaces for different void morphologies of the RVE under PBC is presented in Fig. 8.

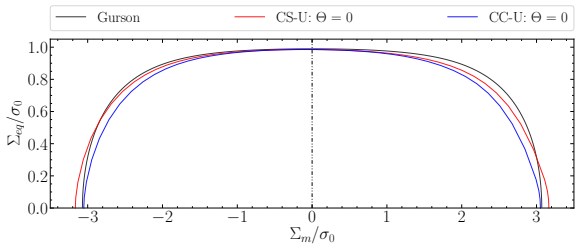

(a) Meridional plane for $\Theta = 0$.

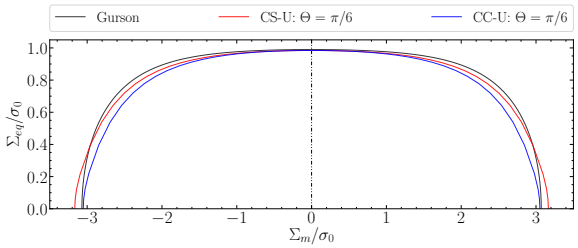

(b) Meridional plane for $\Theta = \pi/6$.

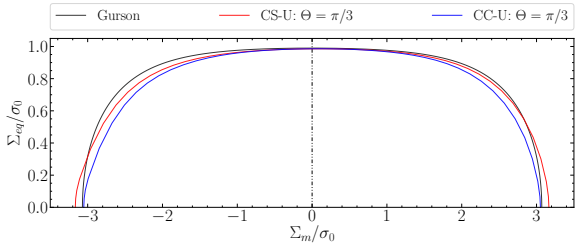

(c) Meridional plane for $\Theta = \pi/3$.

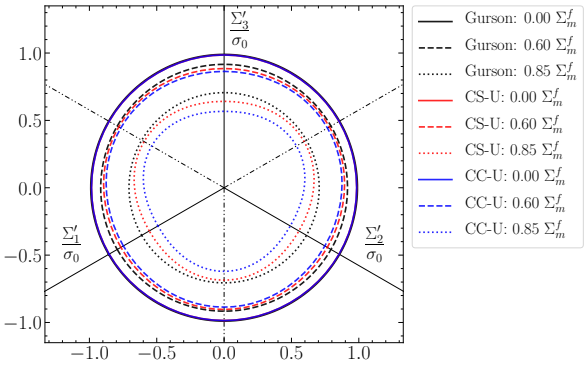

(d) Deviatoric plane for different positive values of $C_f\Sigma_m^f$.

Figure 7: Comparison of the yield surfaces between CS-U and CC-U for $f = 0.01$.

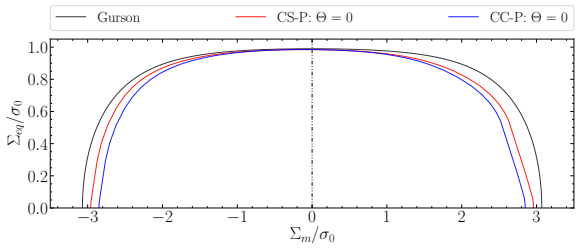

(a) Meridional plane for $\Theta = 0$.

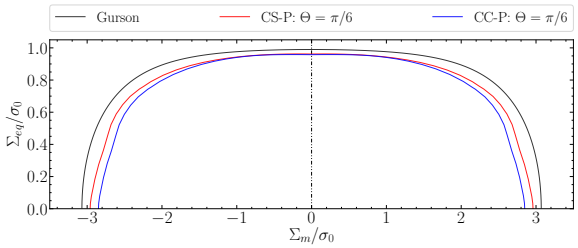

(b) Meridional plane for $\Theta = \pi/6$.

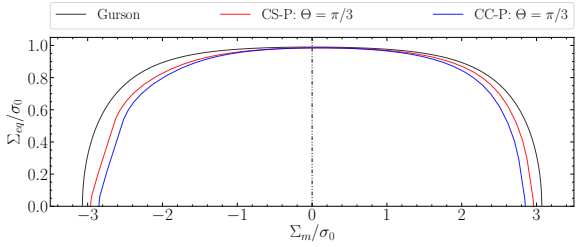

(c) Meridional plane for $\Theta = \pi/3$.

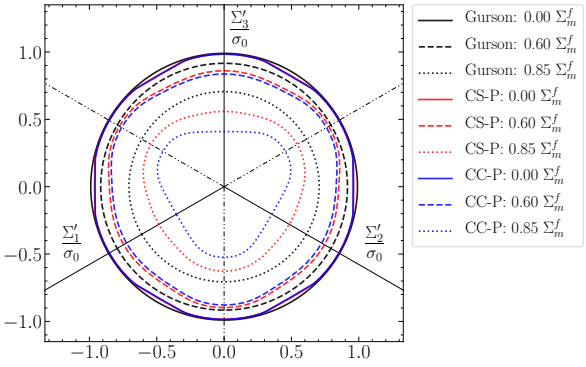

(d) Deviatoric plane for different positive values of $C_f\Sigma_m^f$.

Figure 8: Comparison of the yield surfaces between CS-P and CC-P for $f = 0.01$.

RVE morphology plays an important role in the results of plastic surfaces. The results show a reduction in material strength in the RVE with cubic void when compared to the RVE with a spherical void, mainly for intermediate and high triaxialities. However, the results for different void morphologies are close at low triaxialities for the same boundary condition. The reduction in the material strength of the RVE with a cubic void can be due to: (i) a strong concentration of plastic strains on the internal edges of the cubic void; (ii) the traction-free boundary condition because the surface area

of the spherical void is smaller than the surface area of the cubic void. It is also worth mentioning that the computational results have significant differences compared to the Gurson model. In summary, the Gurson model is an upper bound, except for $T \to 0$ in the RVE with a spherical void under USBC.

4.2 Yield surfaces: influence of the boundary condition imposed on the RVEs

Figure 9 depicts the comparison of yield surfaces for the different boundary conditions imposed on the RVE with spherical void. The comparison of the yield surfaces for the different boundary conditions imposed on the RVE with cubic void is shown in Fig. 10.

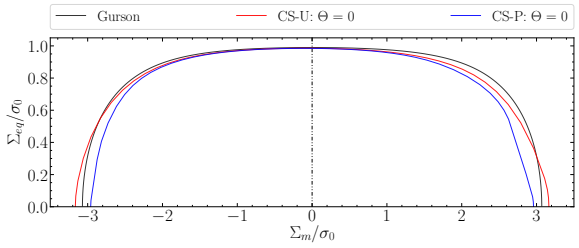

(a) Meridional plane for $\Theta = 0$.

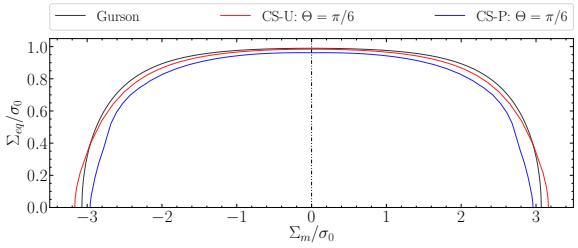

(b) Meridional plane for $\Theta = \pi/6$.

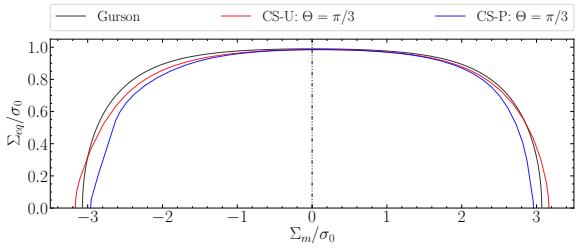

(c) Meridional plane for $\Theta = \pi/3$.

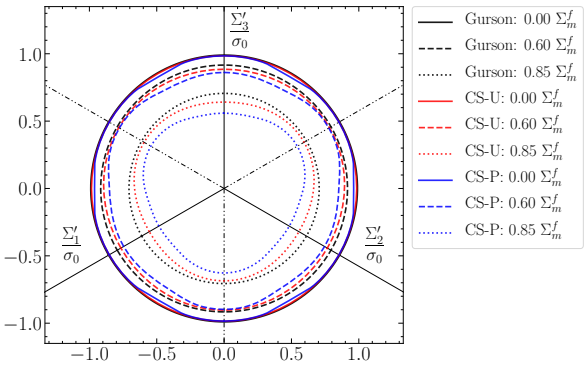

(d) Deviatoric plane for different positive values of $C_f \Sigma_m^f$.

Figure 9: Comparison of the yield surfaces between CS-U and CS-P for $f = 0.01$.

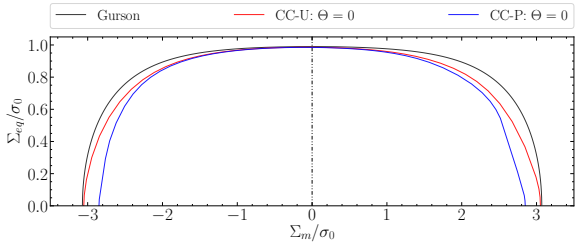

(a) Meridional plane for $\Theta = 0$.

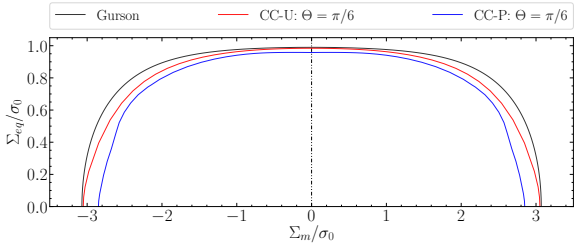

(b) Meridional plane for $\Theta = \pi/6$.

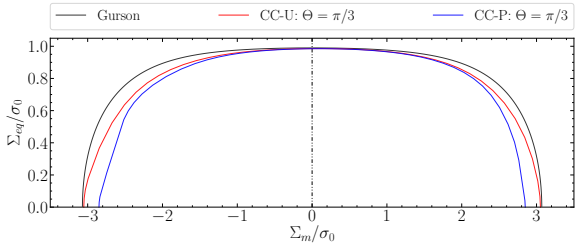

(c) Meridional plane for $\Theta = \pi/3$.

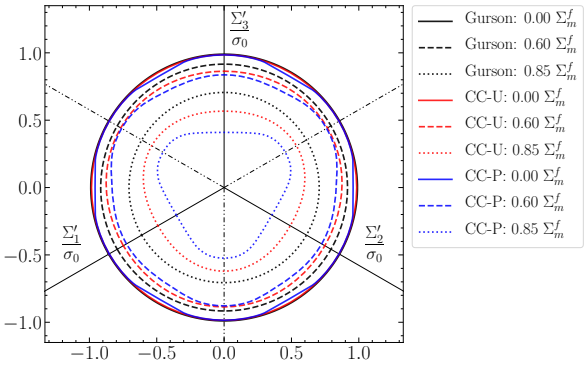

(d) Deviatoric plane for different positive values of $C_f \Sigma_m^f$.

Figure 10: Comparison of the yield surfaces between CC-U and CC-P for $f = 0.01$.

The boundary condition has a strong influence on the results of yield surfaces. Regarding the computational results, USBC provides an upper bound compared to PBC. Therefore, a reduction in material strength is observed for PBC. It is important to mention that PBC allows us to capture the effect of strain localization. In this context, the concentration of plastic deformations observed in RVEs under PBC decreased their strength. The effect of the Lode angle is observed on the geometry of plastic surfaces based on computational results. The Lode angle has more influence for intermediate triaxialities in RVEs under USBC. On the other hand, the influence of the Lode angle is clear for both intermediate and low triaxialities in RVEs under PBC, in which a reduction in material strength is observed for $\Theta = \pi/6$.

5. CONCLUSIONS

In this work, a 3D computational homogenization procedure was explored to investigate complete yield surfaces for isotropic porous ductile media. Numerous numerical simulations were performed to assess the effects of void morphology and boundary conditions imposed on the RVE were addressed in detail. The RVE with a cubic void has lower material strength when compared to the RVE with a spherical void. Thus, numerical results can be reference limits for voids with similar morphology. In addition, the material strength was lower for the RVEs under PBC when compared to the RVEs under USBC.

The results of the numerical simulations showed significant differences in comparison with the analytical model proposed by Gurson (1977). In general, the Gurson model provided an upper bound when compared to the computational results. It is worth mentioning that the numerical simulations allowed us to assess some limitations of Gurson's analytical model: simplified velocity test field; Lode angle disregarded in the formulation; and simplified void morphology.

In the case of USBC imposed on RVEs, the effect of the Lode angle was clear for intermediate triaxialities. For PBC imposed on RVEs, the effect of the Lode angle was evident in both intermediate and low triaxialities. Therefore, the Lode angle had a strong influence on the geometry of plastic surfaces for cubic and spherical void morphologies.

6. ACKNOWLEDGMENTS

The authors would like to gratefully acknowledge Coordination for the Improvement of Higher Education Personnel (CAPES) - Brazil for the financial support.

7. REFERENCES

Benallal, A., Desmorat, R. and Fournage, M., 2014. "An assessment of the role of the third stress invariant in the gurson approach for ductile fracture". *European Journal of Mechanics - A/Solids*, Vol. 47, pp. 400–414.

Bishop, J.F.W. and Hill, R., 1951. "Xlvi. a theory of the plastic distortion of a polycrystalline aggregate under combined stresses". *The London, Edinburgh, and Dublin Philosophical Magazine and Journal of Science*, Vol. 42, pp. 414–427.

Carvalho, R.P., Lopes, I.A.R. and Pires, F.M.A., 2018. "Prediction of the yielding behaviour of ductile porous materials through computational homogenization". *Engineering Computations*, Vol. 35, pp. 604–621.

Dæhli, L.E.B., Hopperstad, O.S. and Benallal, A., 2019. "Effective behaviour of porous ductile solids with a non-quadratic isotropic matrix yield surface". *Journal of the Mechanics and Physics of Solids*, Vol. 130, pp. 56–81.

Fritzen, F., Forest, S., Böhlke, T., Kondo, D. and Kanit, T., 2012. "Computational homogenization of elasto-plastic porous metals". *International Journal of Plasticity*, Vol. 29, pp. 102–119.

Gurson, A.L., 1977. "Continuum theory of ductile rupture by void nucleation and growth: Part i–yield criteria and flow rules for porous ductile media". *Journal of Engineering Materials and Technology*, Vol. 99, No. 1, pp. 2–15.

Khdir, Y.K., Kanit, T., Zaïri, F. and Naït-Abdelaziz, M., 2015. "A computational homogenization of random porous media: Effect of void shape and void content on the overall yield surface". *European Journal of Mechanics - A/Solids*, Vol. 49, pp. 137–145.

Mandel, J., 1971. *Plasticité classique et viscoplasticité*. Springer-Verlag, Udine, Italy.

Santos, W.F., 2021. *Computational modeling of the rupture of elasto-plastic media with initial voids*. Master's degree in civil engineering (structural engineering), São Carlos School of Engineering, University of São Paulo, São Carlos.

Santos, W.F., Ferreira, A.R. and Proença, S.P.B., 2022. "Complete geometric representation of yield surfaces for porous ductile media by a 3d computational homogenization approach: an assessment of the gurson yield criterion". *Journal of the Brazilian Society of Mechanical Sciences and Engineering*, Vol. 44, pp. 1–17.

8. RESPONSIBILITY NOTICE

The authors are solely responsible for the printed material included in this paper.